https://doi.org/10.5194/egusphere-2024-3769
Preprint. Discussion started: 17 December 2024

Marine emissions and trade winds control the atmospheric nitrous oxide in the Galapagos Islands

Timur Cinay[1], Dickon Young[2], Nazaret Narváez Jimenez[3], Cristina Vintimilla-Palacios[3], Ariel Pila Alonso[3], Paul B. Krummel[4], William Vizuete[5], and Andrew R. Babbin[1]

[1]Department of Earth, Atmospheric & Planetary Sciences, Massachusetts Institute of Technology, Cambridge, MA, USA
[2]School of Chemistry, University of Bristol, Bristol, UK
[3]Galapagos Science Center (GSC), Universidad San Francisco de Quito (USFQ) and UNC-Chapel Hill, Puerto Baquerizo Moreno, Galapagos, Ecuador
[4]Centre for Australian Weather and Climate Research, CSIRO Environment, Aspendale, Victoria, Australia
[5]Department of Environmental Sciences Engineering, University of North Carolina, Chapel Hill, NC, USA

Correspondence: Timur Cinay (tcinay@mit.edu) and Andrew R. Babbin (babbin@mit.edu)

Abstract. Nitrous oxide (N_2O) is a potent greenhouse gas emitted by oceanic and terrestrial sources, with its biogeochemical cycle influenced by both natural processes and anthropogenic activities. Current atmospheric N_2O monitoring networks, including tall-tower and flask measurements, often overlook major marine hotspots, such as the eastern tropical Pacific Ocean. We present the first 15 months of high-frequency continuous measurements of N_2O and carbon monoxide from the newly established Galapagos Emissions Monitoring Station (GEMS) in this region. Over this period, N_2O mole fractions vary by approximately 5 ppb, influenced by seasonal trade winds, local anthropogenic emissions, and air masses transported from marine N_2O hotspots. Notably, between February and April 2024, we observe high variability linked to the southward shift of the intertropical convergence zone and weakened trade winds over the Galapagos Islands. Increased variability during this period is driven by stagnant local winds, which accumulate emissions, and the mixing of air masses with different N_2O content from the northern and southern hemispheres. The remaining variability is primarily due to differences in air mass transport and heterogeneity in surface fluxes from the eastern tropical Pacific. Air masses passing over the Peruvian and Chilean upwelling systems — key sources of oceanic N_2O efflux — show markedly higher N_2O mole fractions at the GEMS station.

1 Introduction

Nitrous oxide (N_2O) is a potent greenhouse gas with the fourth-largest effective radiative forcing increase since industrialization, equating to 0.21 $W\,m^{-2}$, and is additionally an ozone-depleting substance in the stratosphere (Forster et al., 2021; Ravishankara et al., 2009). The mean tropospheric growth rate of N_2O between 1995 and 2019 is reported as 0.85 ± 0.03 $ppb\,yr^{-1}$, and is accelerating (Canadell et al., 2021; Dutton et al., 2024; Francey et al., 2003; Prinn et al., 2018). Natural processes dominated by ocean and soil microbial metabolisms, namely denitrification and nitrification, account for the majority of N_2O sources to the atmosphere (Tian et al., 2024). Globally integrated marine N_2O emissions are estimated to be 3.1 – 6.3 $Tg\,N\,yr^{-1}$ (Canadell et al., 2021; Tian et al., 2024) with coastal water contributing to much of this flux (Resplandy et al., 2024). Moreover, data-informed studies tend to report higher marine emissions than biogeochemical

https://doi.org/10.5194/egusphere-2024-3769
Preprint. Discussion started: 17 December 2024

models alone (Resplandy et al., 2024; Tian et al., 2024; Yang et al., 2020). Oxygen minimum zones, characterized by less than 60 $\mu mol\,kg^{-1}$ oxygen content (Stramma et al., 2008), and eastern boundary coastal upwelling systems are hot spots of marine N_2O emissions, accounting for approximately 22 % of oceanic emissions (Yang et al., 2020). Yet the accuracy of these marine estimates has been limited by poor spatial and temporal resolution of ship-based observations. Marine emissions — particularly in the eastern tropical Pacific characterized as one of the largest marine N_2O sources — are further impacted by the El Niño Southern Oscillation (ENSO) through the modulation of coastal nutrient upwelling that supports surface productivity (Babbin et al., 2020; Ji et al., 2019; Thompson et al., 2013, 2019). Reduced upwelling during an El Niño restricts productivity and consequently reduces the magnitude of low oxygen environments in the subsurface where N_2O is produced.

Long-term and high-frequency monitoring of atmospheric greenhouse gases, including N_2O, with flask samples or tall-tower measurements has enabled the exploration of tropospheric growth rates and global emissions estimates with a top-down approach for decades (Hirsch et al., 2006; Patra et al., 2022; Saikawa et al., 2014; Stell et al., 2022; Thompson et al., 2014, 2019; Wells et al., 2015, 2018). Yet, the investigation of regional N_2O surface fluxes or air-sea interface disequilibrium in the literature has highlighted the importance of atmospheric monitoring near emission sources (Babbin et al., 2020; Ganesan et al., 2015, 2020; Jeong et al., 2018; Nevison et al., 2018, 2023; Saboya et al., 2024). Despite the significance of the eastern tropical Pacific as a hotspot of oceanic N_2O emissions with a strong correlation with ENSO (Babbin et al., 2015, 2020; Bange et al., 1996; Ji et al., 2019; Martinez-Rey et al., 2015), there have been no continuous high-frequency atmospheric N_2O monitoring sites in the region (Fig. 1a). Current estimates of N_2O emissions from the area rely on direct measurements during sporadic oceanographic expeditions (Arevalo-Martínez et al., 2015; Buitenhuis et al., 2018; Landolfi et al., 2017; Nevison et al., 1995) and ocean-based statistical or biogeochemical models (McCoy et al., 2023; Suntharalingam et al., 2000; Yang et al., 2020). However, the direct surface flux measurements are temporally and spatially sparse (Bange et al., 2019).

Located in the eastern tropical Pacific Ocean, the Galapagos Islands are situated between two hot spots of oceanic N_2O emissions: (i) the Peruvian and Chilean and (ii) the Costa Rican upwelling systems (Fig. 1a). Therefore, the Galapagos Islands are potentially ideal for monitoring atmospheric N_2O trends in a region where previous direct observations are lacking. Prevailing winds over the Galapagos consist of southeasterly trade winds, transporting air masses from the western coast of South America to the Galapagos most of the year (Forryan et al., 2021). Throughout the year, the temperature remains between 22 – 26 °C, with the maximum precipitation and more stagnant winds observed in February and March (Paltán et al., 2021). During the wet season (January – May), the winds are dominantly easterly due to the southward shift of the intertropical convergence zone (ITCZ) over the eastern Pacific (Risien and Chelton, 2008). Therefore, the seasonality of the winds over the Galapagos creates an opportunity to potentially capture the atmospheric greenhouse gas differences from both hemispheres and record regions of high N_2O emissions in the eastern Pacific.

Despite the significance of the Galapagos Islands' location in the tropical Pacific Ocean for climate research, atmospheric monitoring on the islands has been limited to short-term campaigns focusing on atmospheric pollutants such as particulate matter or ozonesonde deployments at monthly intervals. NASA AERONET (Aerosol Robotic Network) has been active in the Galapagos since 2017, allowing for the identification of baseline aerosol conditions as well as local air pollution episodes (Cazorla and Herrera, 2020). Similarly, other studies have investigated the role of marine aerosols in the local air quality and

https://doi.org/10.5194/egusphere-2024-3769
Preprint. Discussion started: 17 December 2024

their transport from the eastern tropical South Pacific Ocean (Gómez Martín et al., 2013; Sorribas et al., 2015). However, no long-term monitoring studies exist for greenhouse gases, such as N_2O, in the Galapagos.

Here, we present high-frequency and continuous N_2O and CO atmospheric mole fraction observations from the Galapagos Emissions Monitoring Station (GEMS). In this study, we investigate the observed variability in the mole fractions between July 2023 and September 2024 and attribute the variability to changes in local meteorology and regional emissions at synoptic timescales. Similar to previous studies at various atmospheric measurement stations for greenhouse gases and atmospheric pollutants (Ganesan et al., 2013; Grant et al., 2010; Tohjima et al., 2002; Thompson et al., 2009; Zhang et al., 2011), this study aims to advance the understanding of trends in N_2O mole fractions and inform future top-down estimates of regional and global emissions that combine atmospheric transport and inverse models with atmospheric observations.

2 Methods

2.1 Site Description and Sampling Setup

The Galapagos Emission Monitoring Station (GEMS) is located on the island of San Cristóbal in the Galapagos Islands, Ecuador. It is situated in the eastern Pacific Ocean at 0.89562 °S and 89.60866 °W. The instruments are housed in the Terrestrial Ecology Laboratory at the Galapagos Science Center, operated by the Universidad San Francisco de Quito and the University of North Carolina, Chapel Hill. The station is located in the northern part of Puerto Baquerizo Moreno, a city with approximately 7,000 population on San Cristóbal and at the edge of the Galapagos National Park (Fig. 1c). In addition to the GEMS, the Galapagos Science Center is equipped with a weather station that measures temperature, wind speed and direction, relative humidity, and precipitation at 5-minute intervals.

Ambient air is pumped through the sampling line with an inline vacuum pump (Alita Industries, AL-6SA) at 10 $\mathrm{L\,min^{-1}}$ through Monel mesh fitted inside an inverted stainless steel sampling cup. Monel (a nickel-copper alloy) mesh prevents coarser materials from entering the sampling line. The sampling inlet is located on the roof of the Galapagos Science Center at 27 ± 1 m above sea level (17 ± 1 above ground level). Ambient air is pulled through a 1/4" Eaton Synflex 1300 polyethylene-aluminum composite tubing. Inside the laboratory, the air sampling line is heated to 35 °C using a heating cable operated by a temperature controller (CAL Controls, CAL3300). Once in the lab, air samples are pulled from the main Eaton Synflex line using a tee connector attached to a 7-µm stainless steel mesh filter at a rate of 0.1 $\mathrm{L\,min^{-1}}$. The ambient versus calibration air flow is switched via the Picarro Inc. A0311 16-Port Distribution manifold. After the manifold, humidity in the sample is removed using a Nafion™ tubing dryer (Perma Pure Inc.) housed inside a custom temperature-controlled enclosure. Nafion™ dryer is used in reflux mode where out-flowing air from the analyzer is used as a counter purge to dry the inflow (Fig. S1) (Welp et al., 2013). The temperature of the drying box is set to 35 °C using an Omega iSeries temperature controller. Additionally, the air pressure is set to 0.8 atm using a pressure controller (Alicat Inc., PC Series 15-PSIA) inside the drying box. After the drying and pressure control, the air sample is filtered through a 2-µm stainless steel mesh before being introduced to the analyzer. While the 7-µm filter removes any large impurities in the main sampling line before the 16-port distribution manifold, an additional 2-µm filter is necessary upstream of the analyzer to prevent any finer impurities from entering the ultra-clean cavity.

https://doi.org/10.5194/egusphere-2024-3769
Preprint. Discussion started: 17 December 2024

The mole fractions of N_2O, CO, H_2O are measured with a Picarro Inc. G5310 Cavity Ringdown Spectroscopy Analyzer. The flow diagram for air sampling and measurements is illustrated in Fig. S1. All tubing is 316 stainless steel fitted with 316 stainless steel compression fittings (Swagelok). Similar setups have been employed at various atmospheric greenhouse gas monitoring sites (Andrews et al., 2014; Prinn et al., 2018; Stanley et al., 2018).

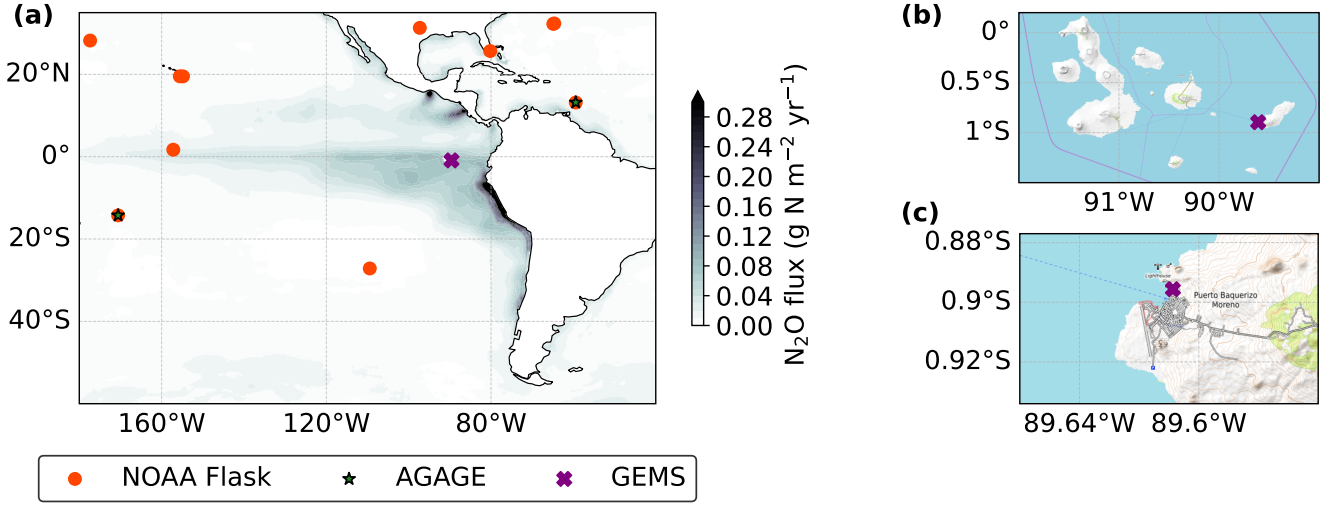

Figure 1. (a) Global atmospheric nitrous oxide monitoring network in relation to the ocean-based and observationally driven nitrous oxide fluxes from Yang et al. (2020). Orange circles signify NOAA Global Greenhouse Gas Reference Network flask-air sample measurement sites (Lan et al., 2024). Green stars signify Advanced Global Atmospheric Gases Experiment (AGAGE) network sites (Prinn et al., 2018). (b, c) Maps of the Galapagos Islands and the island of San Cristóbal, respectively, with the location of the Galapagos Emissions Monitoring Station (GEMS) marked using a purple X. © OpenStreetMap contributors 2024. Distributed under the Open Data Commons Open Database License (ODbL) v1.0.

2.2 Mole Fraction Measurements and Calibrations

The atmospheric composition of the air samples, i.e., the mole fraction of N_2O, CO, H_2O, is measured by a Picarro G5310 Cavity Ringdown Spectroscopy analyzer. Since the air samples are dried prior to measurement, water content is only used to calculate dry air mole fractions and does not represent the humidity of ambient air. The native Picarro G5310 software calculates the dry air mole fraction values using the formulation described by previous studies (Rella, 2010; Reum et al., 2019; Zellweger et al., 2019). No further water vapor corrections are performed as the maximum observed H_2O content was 0.09 % due to the inline Nafion™ tubing dryer. Mole fraction measurements are obtained every 4 – 10 seconds, but 1-minute means and standard deviations are reported. The measurements are calibrated by sampling four calibration tanks at various time intervals.

All the calibration tanks are certified at the NOAA Global Monitoring Laboratory (GML) following the WMO-N_2O_X2006A and WMO-CO_X2014A calibration scales (Hall et al., 2007; Novelli et al., 1991). For this study, each calibration tank is named

https://doi.org/10.5194/egusphere-2024-3769
Preprint. Discussion started: 17 December 2024

based on its use during the calibration process. The standard tank (CC746185; 333.82 ppb N_2O, 136.3 ppb CO) is sampled for 20 minutes daily. A calibration sequence with a high calibration tank (CC746187; 347.54 ppb N_2O, 299.1 ppb CO) and a low calibration tank (CC746176; 326.54 ppb N_2O, 53.9 ppb CO) is performed once per month. A mid-range calibration tank, also referred to as target tank (CC746233; 340.20 ppb N_2O, 163.4 ppb CO) is sampled once per week to evaluate long-term instrument performance. The standard deviation of each measurement session is also used to estimate the repeatability metric for the GEMS sampling and measurement setup, as illustrated in Fig. S2. Based on the average standard deviation of all the measurement sessions for each calibration tank, we report the repeatabilities of N_2O and CO as 0.04 ppb and 0.40 ppb, respectively. The repeatability for N_2O is sufficient to assess the precision of our measurements and is comparable to other high-frequency monitoring stations, with reported repeatabilities between 0.03 and 0.66 ppb (Ganesan et al., 2013; Labuschagne et al., 2018; Lebegue et al., 2016; Stanley et al., 2018). The sampling sequences, instrumental drift calculations, and calibrations are controlled and performed by GCWerks™ software (www.gcwerks.com). The software is widely utilized by various atmospheric monitoring networks such as AGAGE (Prinn et al., 2018) or the UK Deriving Emissions linked to Climate Change (UK DECC) (Stanley et al., 2018; Stavert et al., 2019).

For the calibration calculation, drift corrected mole fraction, χ, is calculated following Equation 1, where χ_{std} refers to the reported value of the standard tank, and m and m_{std} refer to measured dry mole fractions of ambient air and the standard tank, respectively. Furthermore, during calibration sessions, non-linearity calculations are performed based on drift-corrected mole fraction values of high and low calibration tanks. A linear (for N_2O) or quadratic (for CO) relationship between the ratio-to-standard and drift-corrected sensitivity (S_{drift}) is determined for three calibration tanks following Equation 2. These functional forms are selected per common practice (Stanley et al., 2018) because they minimize the R^2 value for the calibration tank non-linearity correction fits, as shown in Fig. S3. As a result, the drift-corrected ambient air mole fraction values are scaled using the determined non-linearity expression for each gas to obtain the reported mole fractions. Post-calibration results from the repeated measurements of these calibration tanks are provided in Fig. S4 to highlight the long-term stability of the measurement and calibration methods.

$$\chi = \chi_{std}\frac{m}{m_{std}} \tag{1}$$

$$S_{drift} = \frac{\frac{\chi_{tank}}{m_{tank}}}{\frac{\chi_{std}}{m_{std}}} \tag{2}$$

2.3 Air Mass Footprint Calculations with FLEXPART Lagrangian Particle Dispersion Model

To estimate the transport history of the air masses sampled at GEMS, we use a Lagrangian particle dispersion model, FLEXPART v10.4 (Flexible Particle Dispersion Model) (Pisso et al., 2019; Stohl et al., 1998, 2005). FLEXPART calculates the location of inert particles in the atmosphere from a Lagrangian perspective, given the wind speeds and direction over time. In this study, we release 50,000 particles every 3 hours from the station at 27 m above sea level and follow them 20 days backward in time within a domain between 40 °W to 121 °W and 50 °S to 31 °N. The meteorology used for the FLEXPART model is the

https://doi.org/10.5194/egusphere-2024-3769
Preprint. Discussion started: 17 December 2024

European Centre for Medium-Range Weather Forecasts (ECMWF) ERA5 reanalysis product with 31 km × 31 km (approximately 0.28125° × 0.28125° for our equatorial site) lateral resolution and 37 vertical pressure levels (Hersbach et al., 2023). The lateral resolution of the FLEXPART model is selected to be the same as ERA5, and the surface layer where the fluxes occur is defined as 0 – 100 m (Pisso et al., 2019; Stohl et al., 2009). The air mass footprints (F; $\mathrm{s\,kg^{-1}\,pmol\,mol^{-1}}$) for each grid cell in the surface layer at a particular period, i.e., the source-receptor-relationship, are calculated from the FLEXPART residence time outputs (Henne et al., 2016; Seibert and Frank, 2004; Stohl et al., 2009). Air mass footprints are calculated until 30 June 2024 as the ECMWF ERA5 reanalysis product's final release is only available with a latency of 2 – 3 months.

We define a regional influence term I, based on the calculated footprints for each 3-hourly release, as shown in Equation 3. This term helps to examine the role of transport from different regions within the domain in modifying the observed N_2O concentrations. The regions considered include (i) the Peruvian and Chilean upwelling systems as previously defined by Yang et al. (2020), (ii) the northern hemisphere, and (iii) a 3-by-3 grid cell area centered on GEMS. All three regions are illustrated in Fig. 2. Each region is indicated by the subscript r, with an associated two-dimensional lateral matrix R to describe the region. In this context, the subscripts i and j indicate latitude and longitude, while t represents the 3-hourly time period when FLEXPART footprints are computed. The matrix R is a binary matrix containing only 0 and 1 values to define a region spatially; therefore, multiplying it with the footprint matrix zeroes out all footprint values outside the defined region. Consequently, the regional influence term $I_{r,t}$ represents the fraction of air masses transported over a specific region relative to the cumulative footprint at a given time. Overall, this metric helps identify how much of the observed N_2O variability can be attributed to air mass transport over each defined region. The histograms for each regional influence metric are provided in Figure S5.

$$I_{r,t} = \frac{\sum_{i,j} F_{i,j,t} \cdot R_{i,j}}{\sum_{i,j} F_{i,j,t}} \tag{3}$$

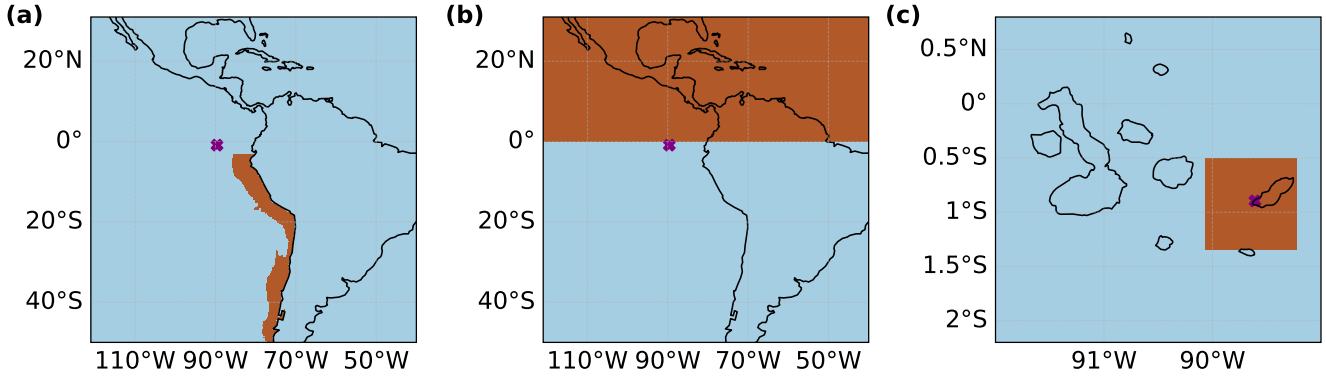

Figure 2. Definitions and histograms of the regional influence metrics for the (a) Peruvian and Chilean upwelling systems (I_{upw}) based on Yang et al. (2020), (b) Northern Hemisphere (I_{NH}), and (c) a local 3-by-3 grid centered on the GEMS region (I_{local}). Each region is highlighted in orange, with the Galapagos Emissions Monitoring Station (GEMS) indicated by a purple X.

https://doi.org/10.5194/egusphere-2024-3769
Preprint. Discussion started: 17 December 2024

3 Results and Discussion

3.1 N_2O and CO Observations in the Galapagos

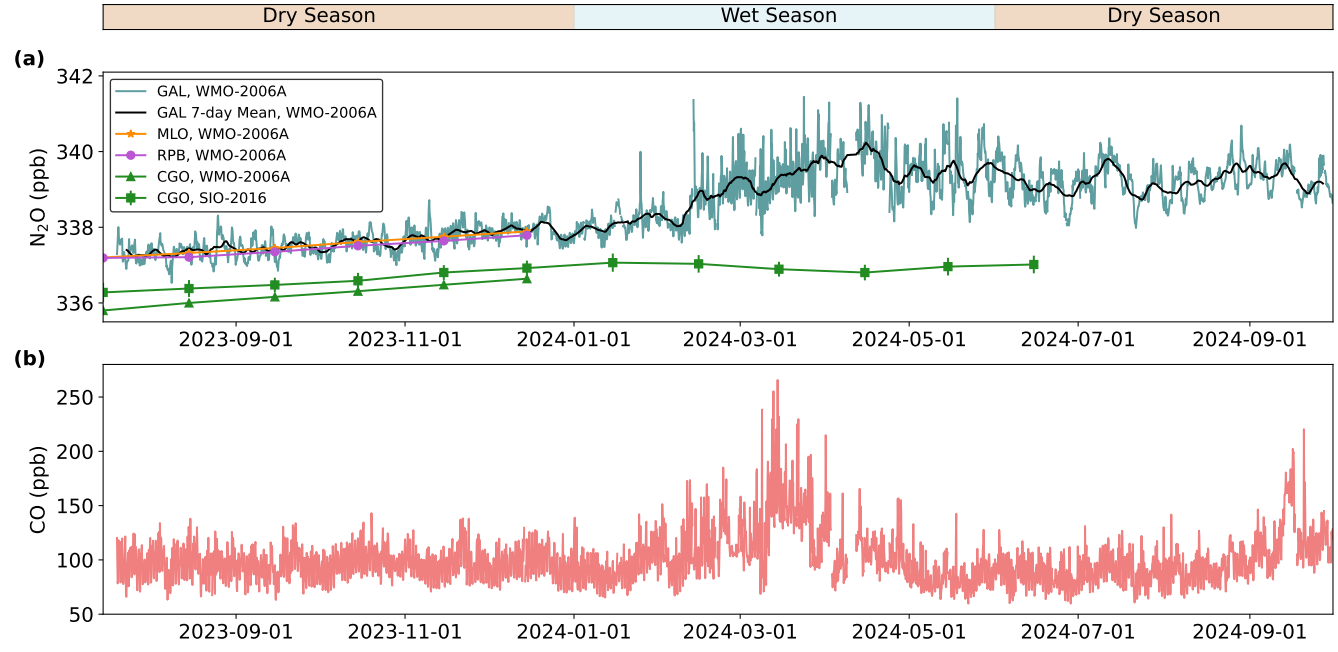

Figure 3. 3-hourly average of (a) nitrous oxide (N_2O) and (b) carbon monoxide (CO) mole fractions at the Galapagos Emissions Monitoring Station, represented with a 3-letter acronym GAL, during the first year of measurements. A 7-day running mean timeseries for GAL N_2O observations is plotted in black. N_2O mole fractions are compared to monthly averages of the stations such as Mauna Loa, Hawaii Observatory (MLO, orange), Ragged Point, Barbados Observatory (RPB, purple), and Kennaook/Cape Grim, Australia Observatory (CGO, green) with two different calibration scales. Measurements calibrated with the NOAA-2006A scale are monthly mean values from NOAA Global Greenhouse Gas Reference Network flask-air sample measurements (Lan et al., 2024). In contrast, CGO, SIO-2016 monthly averages represent the high-frequency atmospheric monitoring station operated by CSIRO and AGAGE networks in Kennaook/Cape Grim (Prinn et al., 2018). Dates are shown in YYYY-MM-DD format. The average 3-hourly standard deviations of N_2O and CO are 0.16 ppb and 3.77 ppb respectively. Since one standard deviation error bars are small compared to the 3-hourly averages, they are not plotted for GAL observations. The color bar above shows the dry season in tan and the wet season in light blue, designated based on climatological precipitation in San Cristóbal (Paltán et al., 2021).

Atmospheric mole fraction of nitrous oxide (N_2O) and carbon monoxide (CO) have been measured continuously since July 2023 at the Galapagos Emissions Monitoring Station. Figure 3 shows a time series of 3-hourly average of the mole fraction measurements. N_2O observations are juxtaposed with monthly mean mole fractions from other high-frequency tall tower or flask measurement sites in the Pacific or tropical Atlantic. Over the first year, the observed N_2O mole fraction in the Galapagos varies between 336.53 and 341.45 ppb with an annual growth rate of 1.82 ± 0.45 $ppb\,yr^{-1}$. This growth rate is calculated

https://doi.org/10.5194/egusphere-2024-3769
Preprint. Discussion started: 17 December 2024

as the average difference in days measured in both 2023 and 2024, and it is comparable to the global growth rate in 2021, which was 1.38 $\mathrm{ppb\,yr^{-1}}$ (Tian et al., 2024). The annual growth rate in the Galapagos is likely overestimated due to the lack of multiple months of continuous data available during both years and the potential impact of emissions-related synoptic $\mathrm{N_2O}$ enhancements. Moreover, the growth rate in the Galapagos is higher compared to the 2010 – 2019 average (Canadell et al., 2021) because it includes interannual variability of natural $\mathrm{N_2O}$ sources in the eastern Pacific Ocean. During 2023, the observed monthly mean $\mathrm{N_2O}$ closely follows the trends illustrated by flask measurements at the Mauna Loa, Hawaii, and Ragged Point, Barbados stations. On the other hand, monthly mean $\mathrm{N_2O}$ mole fractions observed at Kennaook/Cape Grim, Australia, are, on average, 1.30 ppb lower than the Galapagos observations. This difference could be explained by the inter-hemispheric difference in $\mathrm{N_2O}$ mole fractions (Prinn et al., 2018), and low $\mathrm{N_2O}$ fluxes from the Southern Ocean and Antarctic regions over which the air masses sampled at Kennaook/Cape Grim are transported (Wilson et al., 1997). The average $\mathrm{N_2O}$ deviation from a monthly mean during the wet season is 0.73 ppb, whereas it is 0.34 ppb during the dry season. The increase in the variability can be attributed to changes in local and regional wind patterns and meteorology, which will be discussed in more detail later.

Alongside $\mathrm{N_2O}$, CO mole fractions are monitored at GEMS. While 3-hourly averaged CO measurements range between 59 – 266 ppb, no significant annual growth is observed over the Galapagos. The average mole fraction of CO, excluding the highly variable wet season, is 96 ± 22 ppb. This agrees with a previous study that reports the baseline CO mole fraction is 80 ppb with two peaks in March/April and August/September (Cazorla and Herrera, 2020) over the Galapagos based on MOPITT satellite observations. While the increased CO mole fraction in March/April aligns with our observations, no significant increase in CO mole fraction was observed in September 2023. Cazorla and Herrera (2020) attributes the large CO peak in September to the transport of air masses from the Amazon basin during a large biomass-burning season. However, such attributions were supported by air mass back trajectory calculations at 1500 – 5000 m above sea level, whereas the observations at GEMS represent the lower altitude surface mixed layer. However, we observe an increased CO in September 2024, which might be related to large-scale combustion, but further studies are required for such attribution. In addition to its importance for air quality, carbon monoxide mainly indicates local fuel combustion or biomass burning events that could also indicate increased atmospheric $\mathrm{N_2O}$ mole fractions (Bray et al., 2021; Cofer III et al., 1991). Therefore, further discussion of CO variability is only included to support the examination of variability in $\mathrm{N_2O}$ observations in the following sections.

3.2 Diurnal Variability

In Fig. 4, the diurnal cycles of $\mathrm{N_2O}$ and CO mole fractions are represented as the average anomaly from the daily mean at each hour. The amplitude of diurnal variability for $\mathrm{N_2O}$ is 0.16 ppb, approximately 0.05 % of the observed average $\mathrm{N_2O}$ mole fraction. However, $\mathrm{N_2O}$ diurnal cycle standard deviation is much larger than the amplitude due to strong synoptic variability in $\mathrm{N_2O}$ observations. The peak mean $\mathrm{N_2O}$ anomaly is observed at 12:00 UTC (06:00 local time), and the lowest mean $\mathrm{N_2O}$ anomaly is observed at 22:00 UTC (17:00 local time). The diurnal trend is approximately sinusoidal with decreasing $\mathrm{N_2O}$ during the day and increasing at night. Compared with the diurnal cycle of meteorological variables such as temperature and wind speed (Fig. S6 & S7), the decrease in $\mathrm{N_2O}$ during the day is associated with warmer surface temperatures and increased mean wind speed, hence a thicker surface boundary layer. As the boundary layer expands early in the morning, low $\mathrm{N_2O}$

https://doi.org/10.5194/egusphere-2024-3769
Preprint. Discussion started: 17 December 2024

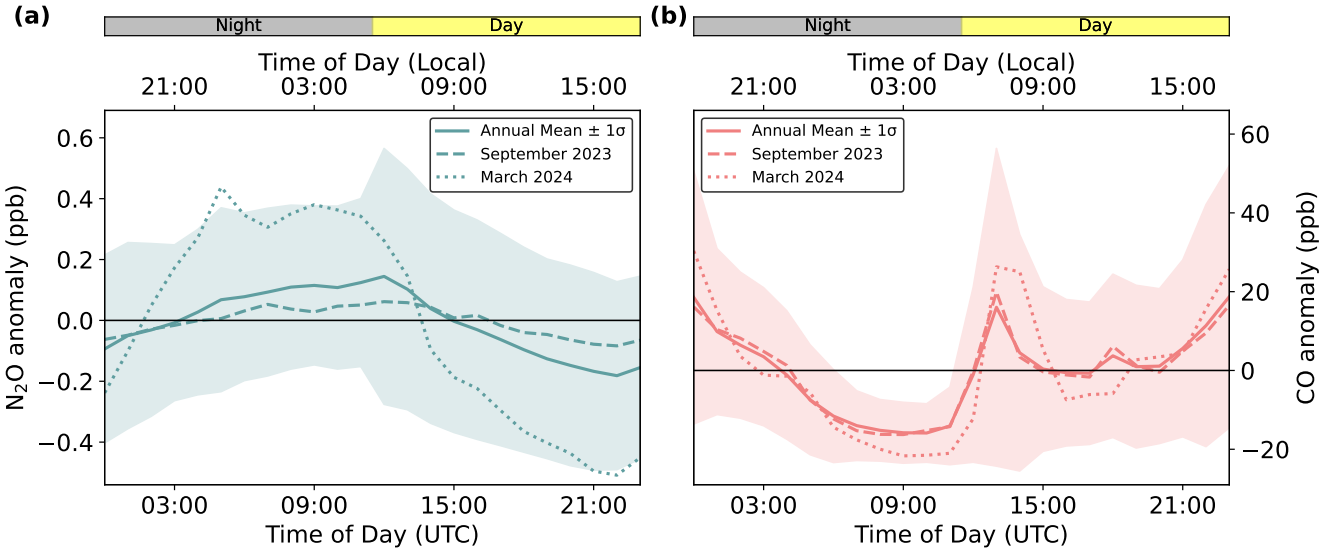

Figure 4. Observed diurnal cycle in (a) nitrous oxide (N_2O) and (b) carbon monoxide (CO) at GEMS. The diurnal cycle is represented as the hourly anomaly from the daily mean mole fractions. Shading signifies one standard deviation range for the overall mean. The solid black line represents zero anomaly. The time is reported in UTC to match the time zone used for reporting the mole fraction observation. The local time in the Galapagos is GMT-6. The color bar above each panel indicates daytime in yellow and nighttime in gray. No significant variation in day length is observed in the Galapagos due to its proximity to the equator.

air from higher altitudes mixes with the surface, resulting in dilution of N_2O during the day. However, the boundary layer shrinks and is stable at night, allowing for the accumulation of N_2O with a mean slope of 0.02 $\mathrm{ppb\,hr^{-1}}$. Given the mean boundary layer height estimated from ERA5 reanalysis (Hersbach et al., 2023) at this location is 529 m, a surface N_2O flux of 0.12 $\mathrm{g\,N\,m^{-2}\,yr^{-1}}$ is necessary to sustain the observed mean increase in nighttime N_2O. Yang et al. (2020) reports approximately 0.1 $\mathrm{g\,N\,m^{-2}\,yr^{-1}}$ N_2O flux from the ocean immediately surrounding the Galapagos (Fig. 1a). Therefore, the adjacent ocean is likely the dominant source of local N_2O emissions, leading to mean nighttime accumulation. Previous studies estimating greenhouse gas fluxes within the surface boundary layer show that such flux estimates are highly dependent on assumptions about the boundary layer dynamics and accurate mole fraction measurements in the free troposphere above the boundary layer (Griffis et al., 2013; Zhang et al., 2014). While such measurements are not currently available at the GEMS site, this does not prevent the attribution of sources across the ocean via other methods in the following sections.

The N_2O diurnal cycle also varies seasonally between the dry and wet seasons. Compared to September 2023, March 2024 exhibits a larger diurnal variability with an amplitude reaching 0.40 ppb. Additionally, the peak N_2O is observed earlier in the morning during the wet season compared to the annual mean. Despite the change in the N_2O diurnal cycle amplitude seasonally, the diurnal cycles of temperature, wind speed, and relative humidity remain unchanged between the two seasons. However, the diurnal cycle of the wind direction has a larger amplitude in March 2024 compared to September 2023 (Fig. S6). A likely cause for this trend is the seasonal weakening of southeasterly winds over the Galapagos, allowing for more variable

https://doi.org/10.5194/egusphere-2024-3769
Preprint. Discussion started: 17 December 2024

circulation, as illustrated in Fig. 5. Thus, the observed seasonal N_2O is mainly driven by the wind direction and transport history of the air masses. It is important to note that the mean observed temperature in March 2024 (Fig. S6) is approximately 1°C higher than the March climatology reported by Paltán et al. (2021), likely due to the 2023–2024 El Niño event. As a result, climatological seasonal differences may be less pronounced, and more years of observation are needed to draw a more definitive conclusion.

Compared to N_2O, the diurnal cycle of CO has a larger amplitude of 17.3 ppb, corresponding to 18% of the background CO mole fractions. Unlike N_2O, CO has two peaks at 13:00 UTC (7:00 local time) and 00:00 UTC (18:00 local time). These peaks correspond to daily commuting hours and high tourism activity in Puerto Baquerizo Moreno and are likely due to increased anthropogenic emissions at these times. As the GEMS station is located in the northern part of the population center with dominant southeasterly winds, the air masses are likely to accumulate such emissions. Nonetheless, a simultaneous increase in N_2O is not observed at these daily commuting hours, suggesting negligible local anthropogenic N_2O emissions. Additionally, no seasonal difference in the diurnal cycle is observed in CO despite the change in wind directions during the wet season, implying a minimal marine source and confirming the assumption that N_2O variability is dictated by air mass transport history whereas CO conveys a signal of local combustion.

3.3 Seasonality and Atmospheric Circulation

The transport history of the air masses sampled at Galapagos is critical for understanding variability observed in N_2O mole fraction because the surface fluxes are distributed heterogeneously in space (Arevalo-Martínez et al., 2015; Buitenhuis et al., 2018; Nevison et al., 1995; Suntharalingam et al., 2000; Yang et al., 2020). The long atmospheric residence time of N_2O, 116 ± 9 yr (Prather et al., 2015) and lack of N_2O sinks in the troposphere (Tian et al., 2024) allows for lower tropospheric N_2O mole fractions to be set solely by mixing or net surface exchange. Therefore, any variability in the N_2O is linked to either temporal variability in surface fluxes or the changes in the air mass transport history. As a regional product of wind speed and direction is required to generate such transport histories, i.e., footprints, we investigate the trends and variability in ERA5 and observed wind patterns over the Galapagos. We use the ECMWF ERA5 reanalysis product for the air mass footprint calculations as it assimilates various direct observations and forecast models to accurately represent the atmospheric circulation globally (Hersbach et al., 2023). Fig. 3 illustrates that observed N_2O is higher during the wet season compared to the dry season, with more substantial variability. Furthermore, local observations in Fig. 5 suggest that there is a shift from strong, on average 2.01 ± 0.91 $\mathrm{m\,s^{-1}}$ (1 s.d.), southerly winds to weaker, on average 0.67 ± 0.88 $\mathrm{m\,s^{-1}}$, easterly winds over the Galapagos. On the other hand, ERA5 reports higher wind speed compared to direct observations, with a mean of 5.83 ± 0.89 $\mathrm{m\,s^{-1}}$ in September 2023 and a mean of 2.62 ± 0.94 $\mathrm{m\,s^{-1}}$ in March 2024. The difference is mainly justifiable because the ERA5 product estimates average winds over a 0.25° × 0.25° at the surface. In contrast, the GSC observations are collected at a specific point within that grid cell. Similarly, wind directions between ERA5 and the GSC observations differ slightly, likely due to the impact of topography on the atmospheric circulation over the single observational point in a grid cell mainly dominated by an ocean surface. Nonetheless, the reanalysis product captures the seasonality in the winds with a

https://doi.org/10.5194/egusphere-2024-3769
Preprint. Discussion started: 17 December 2024

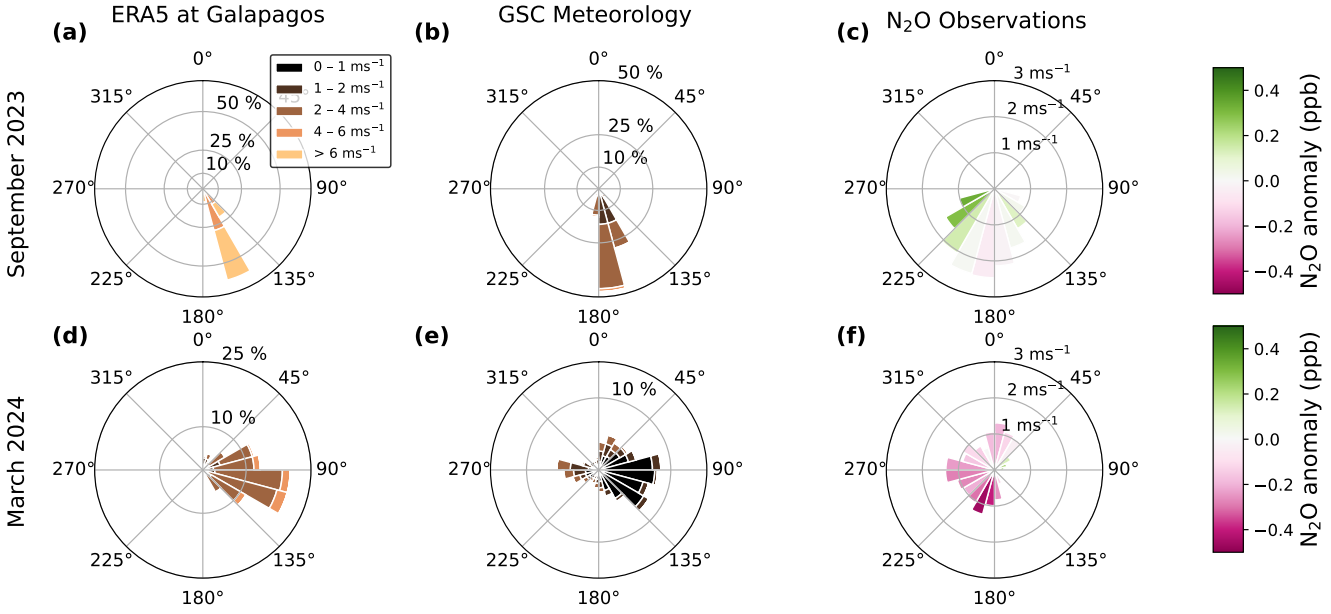

Figure 5. Observed vs. European Centre for Medium-Range Weather Forecasts (ECMWF) ERA5 surface wind speeds and directions in the Galapagos. Panels (a) & (d) show the monthly winds from ECMWF ERA5 for the grid cell where GEMS is located (Hersbach et al., 2023). Panels (b) & (e) illustrate the winds observed at GEMS, collected and reported by the Galapagos Science Center (GSC). Wind speed is indicated by the color bar, and the radial height of each bar represents the frequency of observations. Panels (c) & (f) show the mean nitrous oxide mole fraction anomaly from a 7-day running mean. The color bar indicates the mole fraction anomaly, and each bar's radial height represents the associated wind speed. Wind directions are represented by the angle of each bar around the polar axis. Panels (a) – (c) correspond to observations in September 2023, whereas panels (d) – (f) correspond to those in March 2024.

shift from strong southeasterly to weaker easterly winds, making the ERA5 product a suitable meteorological input for the atmospheric transport model discussed in Section 2.3.

Although Fig. 5(c) & (f) suggest that there is no significant relationship between the N_2O mole fractions and the observed wind direction and speed, it is evident that these observed features are more variable in March 2024 compared to September 2023 due to the southward shift of the ITCZ to the latitude of the Galapagos in the eastern Pacific. Nevertheless, air mass footprints calculated using the FLEXPART model are a better tool than the observed wind directions to examine the variability in the N_2O mole fraction anomalies as they represent the history of air masses over different surfaces where the emissions would occur. Figure 6 shows the GEMS's calculated air mass back trajectory footprints between July 2023 and June 2024, as described in Section 2.3. Between August and December, the air masses sampled at the station are dominantly transported over the western coast of South America, where intense marine N_2O fluxes have been reported (Arevalo-Martínez et al., 2015; Buitenhuis et al., 2018; Nevison et al., 1995; Suntharalingam et al., 2000; Yang et al., 2020). Additionally, most of the air masses enter the domain from the southern and southwestern boundaries, where air masses are likely to have low N_2O due

https://doi.org/10.5194/egusphere-2024-3769
Preprint. Discussion started: 17 December 2024

to the lack of significant marine emissions in the central Pacific and Southern Oceans (Buitenhuis et al., 2018; Thompson et al., 2014; Yang et al., 2020). Starting in December, air masses transported from the northern hemisphere are also sampled at the station, with the peak northern hemispheric influence in March 2024. Due to inter-hemispheric differences in N_2O mole fractions, more northern hemispheric influence in the later periods is likely the reason for increased baseline between February and April 2024, setting the overall seasonal difference in N_2O.

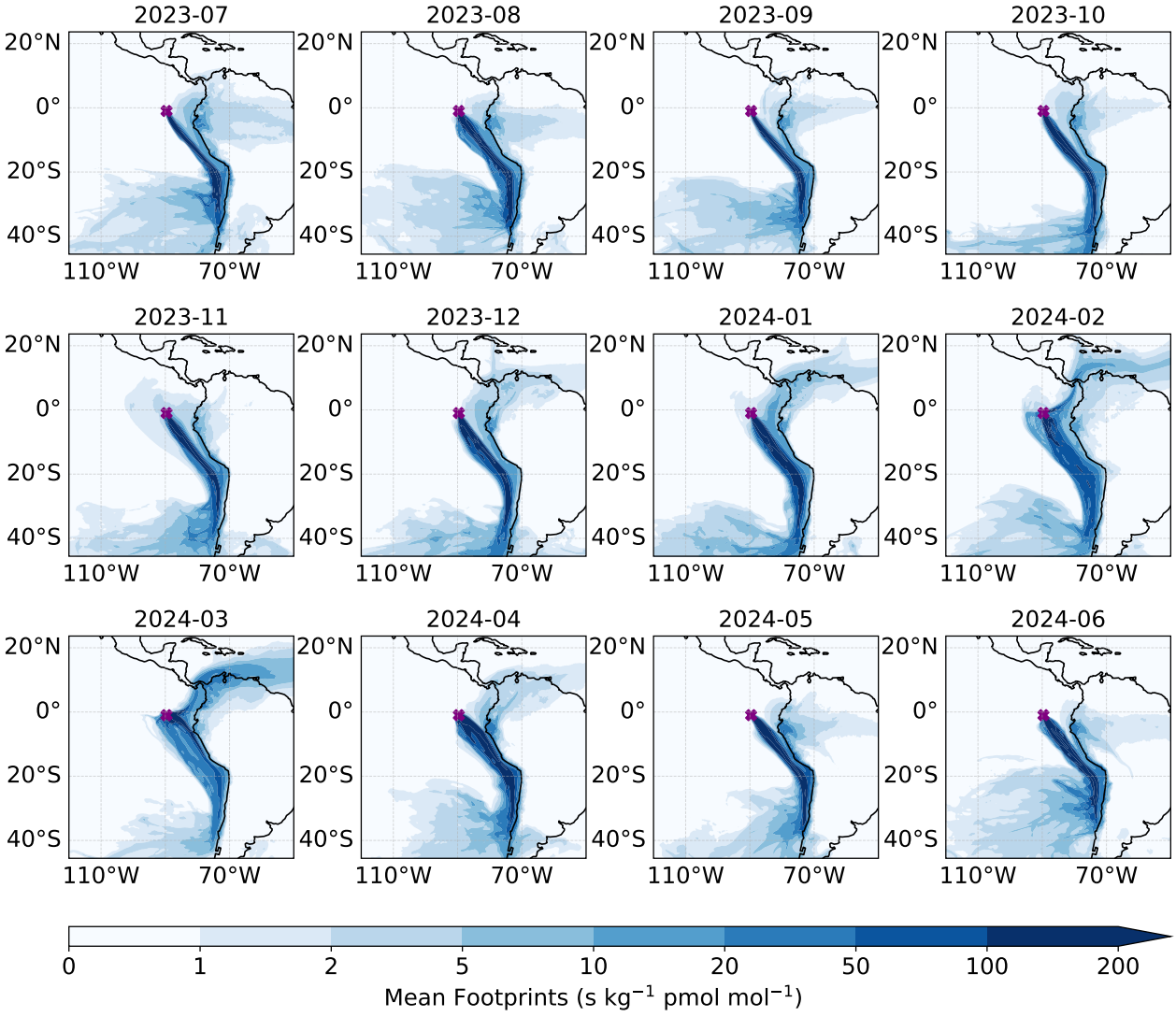

Figure 6. Monthly mean air mass back trajectory footprints simulated by the FLEXPART model and ERA5 reanalysis meteorology between July 2023 and June 2024. The footprints are derived from the total residence time of particles released at the Galapagos Emissions Monitoring Station in each grid cell at the surface (0 – 100 m) throughout 20-day back trajectories. The Galapagos Emissions Monitoring Station is marked with a purple X.

https://doi.org/10.5194/egusphere-2024-3769
Preprint. Discussion started: 17 December 2024

3.4 Local Nitrous Oxide Emissions

In addition to the seasonal and diurnal effects, the observed magnitude and variability of N_2O in the Galapagos can be attributed to the variability of fluxes over the eastern Pacific and South America. However, these analyses cannot account for local emissions in San Cristóbal, originating in the same grid cell as the sampling location. Therefore, independent estimates of local emissions are needed. Currently, there are only a limited number of studies estimating the greenhouse gas emissions from the Galapagos, and they are restricted to annual emissions (Mateus et al., 2023), reporting 6.2 metric tons of N_2O emissions annually, dominated by marine transportation and aviation sectors. Even though 6.2 metric tons of N_2O emissions comprise <0.001% of the estimated marine emissions from the eastern tropical Pacific (Yang et al., 2020), they can enhance N_2O mole fractions significantly if episodic and close to the measurement site. Thus, in Fig. 7, we explore three different indicators to determine potential N_2O enhancements associated with the local emissions close to the sampling location: (i) CO enhancement, (ii) wind stagnation, and (iii) a local regional influence metric (I_{local}).

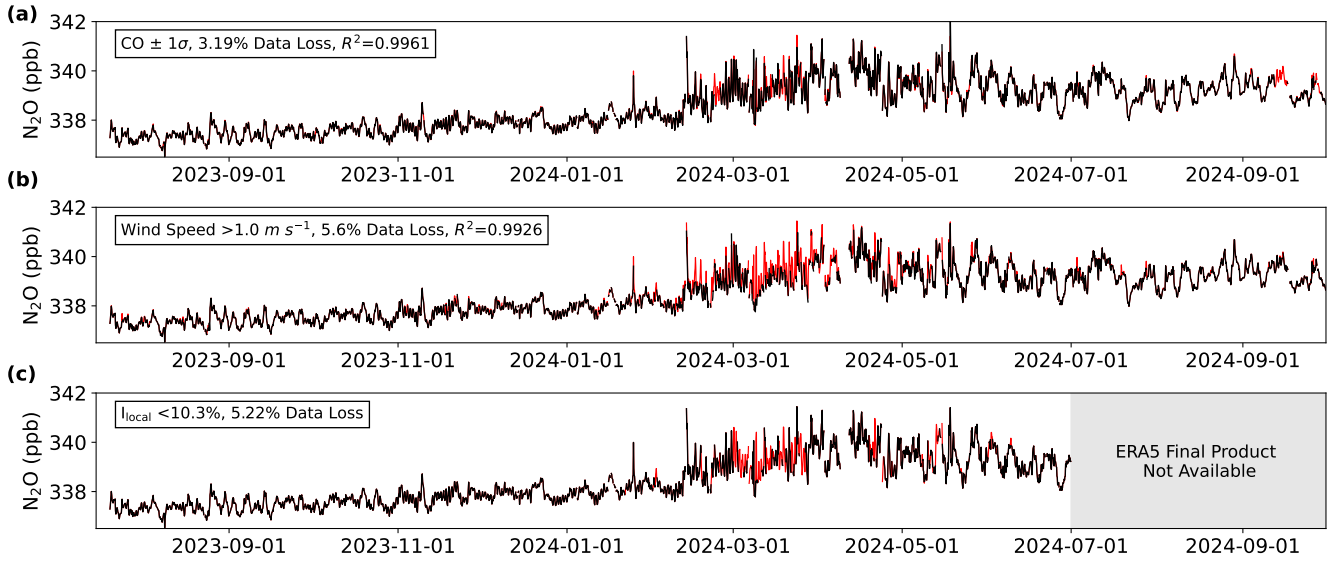

Figure 7. 3-hourly averaged nitrous oxide mole fractions filtered based on (a) carbon monoxide mole fractions, (b) observed wind speed and (c) local regional influence metric (I_{local}). Filters are applied to the original 1-minute average data. The black lines represent the nitrous oxide observations that satisfy the conditions described in the legend, whereas the red lines are the observations that are filtered out.

Firstly, CO is an indicator of combustion activities associated with transportation, tourism, and energy generation as it is a by-product of combustion, similar to N_2O (Cofer III et al., 1991; Watson et al., 1990), and any large-scale and episodic combustion events could simultaneously increase both N_2O and CO. To filter out such events, we use a two-standard deviation range around the monthly mean CO mole fraction. The filter rarely detects significant co-enhancement of N_2O and CO, and only a small portion, 3.19 %, of N_2O observations are filtered. Some 3-hourly averages are adjusted due to the filtering of individual observations, resulting in a pre-filter vs. post-filter R^2 value of 0.9961. Secondly, we use a wind speed filter based

https://doi.org/10.5194/egusphere-2024-3769
Preprint. Discussion started: 17 December 2024

on the direct measurements at the GSC, assuming that slow wind speeds may allow longer residence time over the island and accumulate more local emissions. Wind speeds below 1.0 $\mathrm{m\,s^{-1}}$ are filtered out, resulting in a 5.6 % loss of 3-hourly average observations and a pre-filter vs. post-filter R^2 value of 0.9926. The filter mainly affects the N_2O enhancements between February and April 2024.

Lastly, the local influence filter considers both the wind speed and direction to estimate how stagnant the air masses are close to the sampling site. The filter is defined by a 3-by-3 grid cell area centered on GEMS as the local region and calculates the regional influence (I_{local}) following Equation 3. The distribution of calculated I_{local} values is presented in Fig. S5. Due to the dominance of trade winds in the region, the I_{local} is low, with a median of 5.1 %. Since 10.3 % represents the 95th precentile of I_{local}, we chose this critical value for filtering stagnant air masses with high local influence. Similar filtering of local effects based on transport model footprints is implemented commonly (An et al., 2024; Ganesan et al., 2015; Lunt et al., 2021; Saboya et al., 2024), with the specific critical value depending highly on the mean circulation and topography around the sampling sites. This filter removes 5.22 % of 3-hourly average N_2O mole fractions, mainly during late March and early April 2024. R^2 is arbitrary for this filter, as the footprint calculations are only performed at 3-hour intervals. Overall, all three filters mainly remove a small number of enhanced N_2O mole fractions during the wet season over the Galapagos. When combined, these filters suggest that the weakening and directional changes in the winds due to the seasonality of the ITCZ play a critical role in setting the time periods when local anthropogenic emissions might mask any regional marine emissions.

3.5 Nitrous Oxide Enhancements and Marine Emissions

After applying the three filters shown in Fig. 7 to exclude air masses potentially affected by local emissions, we examine the contribution of regional emissions from marine hotspots to the variability in observed N_2O. Given the strong oceanic fluxes from the Peruvian and Chilean upwelling systems in the eastern tropical Pacific (Arevalo-Martínez et al., 2015; Buitenhuis et al., 2018; Nevison et al., 1995; Suntharalingam et al., 2000; Yang et al., 2020), we calculate the upwelling influence (I_{upw}) as described in Section 2.3. The boundaries for the Peruvian and Chilean upwelling regions are defined based on Peru and Chile's exclusive economic zones and surface flux magnitudes, following Yang et al. (2020), and are shown in Fig. 2. Similarly, we calculate the northern hemispheric influence (I_{NH}) to assess the impact of air mixing from the northern hemisphere on N_2O variability. The distributions of I_{upw} and I_{NH} throughout the observation period are provided in Fig. S5. Generally, air masses transported over the Peruvian upwelling system also pass over the Chilean upwelling system, as shown in Fig. 6 for October 2023. However, not all air masses that pass over the Chilean upwelling system travel over the Peruvian upwelling system. Given the similar mechanisms controlling fluxes in both regions, we combined the Peruvian and Chilean upwelling systems into a single region. To explore the role of these regional influences on N_2O variability, we compare them to the N_2O anomaly, calculated as a deviation from the 7-day running mean (Fig. 8).

From Fig. 8, we observe that air masses influenced by upwelling regions are generally associated with a significant positive N_2O anomaly relative to the 7-day mean. Air masses with high upwelling influence ($I_{upw} > 0.4$) and low northern hemisphere influence ($I_{NH} < 0.18$) exhibit a mean N_2O anomaly of 0.15 ± 0.38 ppb. These samples are predominantly transported over the Peruvian and Chilean upwelling zones, particularly near coastal regions where the most intense upwelling occurs (Fig. 7b).

https://doi.org/10.5194/egusphere-2024-3769
Preprint. Discussion started: 17 December 2024

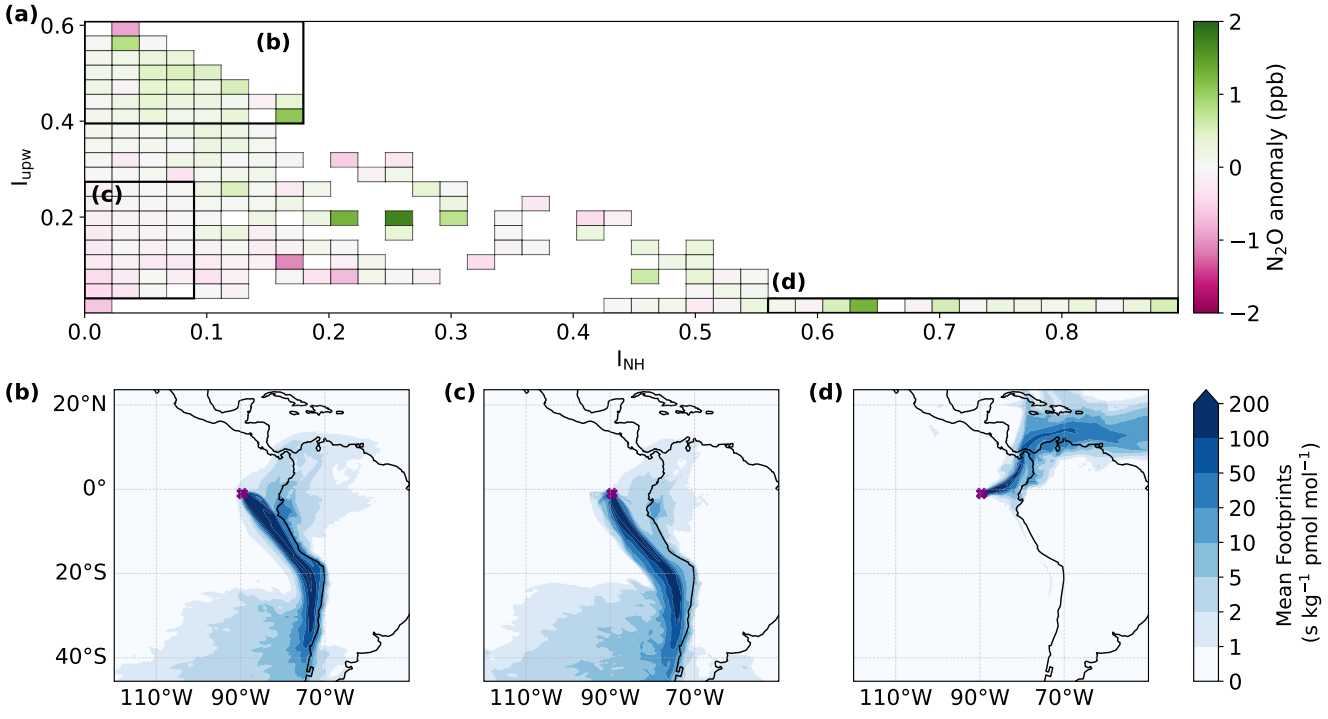

Figure 8. Attribution of observed nitrous oxide (N_2O) enhancements to air mass source regions, specifically the Peruvian and Chilean upwelling systems and the northern hemisphere. Panel (a) shows the mean anomaly of N_2O mole fractions relative to a 7-day mean, binned by varying levels of influence from upwelling systems (I_{upw}) and the northern hemisphere (I_{NH}). Definitions of the upwelling systems and northern hemisphere regions are provided in Fig. 2, and regional influences are calculated using Equation 3. Mean footprint maps are shown under varying influences: (b) high upwelling, low northern hemisphere; (c) low upwelling, low northern hemisphere; (d) low upwelling, high northern hemisphere. Panel (a) shows bin locations corresponding to Panels (b) – (d).

Although high I_{upw} correlates with more positive N_2O anomalies, the observed standard deviation exceeds twice the mean value, suggesting that variability in surface fluxes may significantly influence N_2O fluctuations, in addition to atmospheric transport effects.

In contrast, air masses with $I_{upw} < 0.09$ and $I_{NH} < 0.27$ display a mean N_2O anomaly of -0.16 $\pm$ 0.26 ppb, indicating that these air masses, largely transported by southeasterly winds over the eastern tropical Pacific Ocean, remain offshore from the high N_2O emission zones within the Peruvian and northern Chilean upwelling systems (Fig. 7c). The extent of the upwelling region and the magnitude of associated fluxes likely play a critical role in determining the mean N_2O levels in this low upwelling system and low northern hemispheric influence regime. The large standard deviation around this mean may be attributed to spatial variability that deviates from the defined boundaries of the upwelling systems, as outlined by Yang et al. (2020). For instance, the extent and intensity of N_2O fluxes can be significantly altered during the El Niño events due to a more stratified surface ocean in the eastern Pacific. Thus, while synoptic-scale N_2O variability is modulated by air mass

https://doi.org/10.5194/egusphere-2024-3769
Preprint. Discussion started: 17 December 2024

transport pathways driven by winds, spatial heterogeneity in marine fluxes along the upwelling zones is essential for capturing the observed variability.

Lastly, air masses with $I_{upw} < 0.03$ and $I_{NH} > 0.56$ show a mean N_2O anomaly of 0.21 ± 0.53 ppb. These air masses with negligibly low upwelling system influence and high northern hemispheric influence do not overlap with any significant oceanic N_2O sources; however, emissions from northwestern South America and southern Central America could play a role in modifying the N_2O anomaly based on the footprint distribution (Fig. 7c). Additionally, increased N_2O in the northern hemisphere compared to the southern hemisphere (Prinn et al., 2018) could result in higher observed N_2O at the Galapagos during periods of high northern hemispheric influence.

4 Conclusions

This study addresses a significant gap in long-term monitoring of atmospheric N_2O content in the eastern tropical South Pacific, a region strongly influenced by substantial marine N_2O emissions and climate variability modes like ENSO. We presented continuous, high-frequency N_2O and CO measurements collected at the Galapagos Emissions Monitoring Station (GEMS) from July 2023 to September 2024, located in San Cristóbal, Galapagos Islands, Ecuador. Our findings highlight that N_2O variability in this region is strongly driven by seasonal trade winds, which regulate air mass mixing between the northern and southern hemispheres and the air mass transport over marine nitrous oxide hot spots. During the wet season, we observed elevated variability in N_2O and CO due to reduced wind speeds that allowed local pollution to accumulate before reaching the sampling site. By implementing filters based on CO measurements, wind speed, and air mass transport models, we minimized the potential influence of these local pollution events, ensuring an accurate representation of regional N_2O trends. A comparison of diurnal cycles further suggests that local anthropogenic emissions do not impact N_2O variability except for a limited number of pollution events during the wet season. Prominently during the dry season, air masses with high influence from the Peruvian and Chilean upwelling systems exhibited elevated N_2O levels at GEMS, linking marine N_2O emissions to atmospheric concentrations at this site. Additionally, the analysis of regional influences clarified that the spatial and temporal variability in surface N_2O emissions could strongly modify the observed N_2O, underscoring the heterogeneity of fluxes in the eastern Pacific and the need for continued continuous measurements. While this study provides valuable insights, the current methods cannot provide more robust estimates of marine and terrestrial fluxes in the region. Follow-up studies with inverse modeling approaches are needed to further dissect the impacts of spatial and temporal heterogeneity on atmospheric N_2O variability in this region.

Data availability. N_2O and CO mole fraction measurements at the Galapagos Emissions Monitoring Station (GEMS) are available from BCO-DMO https://www.bco-dmo.org/dataset/917743 and can be accessed through gems.mit.edu. Galapagos Science Center weather station data is available from https://usfq.shinyapps.io/weathergsc/. NOAA GML CCGG nitrous oxide flask measurements are publicly available on https://gml.noaa.gov/ccgg/. AGAGE Network CGO station nitrous oxide measurements are publicly available through https://www-air.

https://doi.org/10.5194/egusphere-2024-3769
Preprint. Discussion started: 17 December 2024

larc.nasa.gov/missions/agage/. ECMWF ERA5 reanalysis product is available on Copernicus Climate Data Store on https://cds.climate.
355 copernicus.eu/.

Author contributions. T.C., A.R.B.: conceptualization of the project; T.C., A.R.B, D.Y., N.N.J, C.V.P., A.P.A, W.V.: station establishment and measurements; D.Y., N.N.J., P.B.K,: providing additional data; T.C., D.Y.: data analysis and calibration; T.C., A.R.B: writing of the first draft; T.C., A.R.B., D.Y.,N.N.J, C.V.P., A.P.A, P.B.K, W.V.: editing and reviewing

Competing interests. The authors declare that they have no conflict of interest.

360 *Acknowledgements.* We acknowledge the entire Galapagos Science Center (GSC) team's support in establishing and maintaining the measurement station and coordinating sampling permits. We want to thank Stephen J. Walsh and Francisco Laso for establishing initial communication with the GSC. We acknowledge the Kennaook/Cape Grim Observatory, AGAGE, and CSIRO networks for providing monthly mean observations in Fig. 2. AGAGE is supported principally by the National Aeronautics and Space Administration (USA) grants to the Massachusetts Institute of Technology and the Scripps Institution of Oceanography. Kennaook/Cape Grim is operated and managed by the
365 Australian Bureau of Meteorology, with the science program undertaken in collaboration with CSIRO. We thank NOAA GML Carbon Cycle Cooperative Global Air Sampling Network for making nitrous oxide flask measurement data available to us. We acknowledge ECMWF and Copernicus Climate Change and Atmospheric Monitoring Services for making ERA5 reanalysis products publicly available. We thank Duane Kitzis from NOAA Global Greenhouse Gas Reference Network for helping us obtain calibration standards. The study benefited from conversations with Susan Solomon, Daniele Bianchi, Ronald C. Cohen, Kristie A. Boering, Ronald G. Prinn, Shuhei Ono, and Ray F. Weiss. This
370 work was funded by NSF Grant OCE-2138890 to A.R.B. We are grateful for MIT's Earle A Killian III and Waid Lee Seed Fund for initial funding to purchase Picarro G5310 analyzer awarded to A.R.B. and the MIT Phillips Fellowship in Environmental Sustainability awarded to T.C. Air sampling conducted in the Galapagos is performed per permits No. PC-84-22 and No. PC-82-23, issued by the Galapagos National Park. This work is dedicated to Laura Papa Babbin, who inspired her son to pursue his dreams wherever they took him.

https://doi.org/10.5194/egusphere-2024-3769
Preprint. Discussion started: 17 December 2024

References

An, M., Prinn, R. G., Western, L. M., Zhao, X., Yao, B., Hu, J., Ganesan, A. L., Mühle, J., Weiss, R. F., Krummel, P. B., et al.: Sustained growth of sulfur hexafluoride emissions in China inferred from atmospheric observations, Nature Communications, 15, 1997, 2024.

Andrews, A., Kofler, J., Trudeau, M., Williams, J., Neff, D., Masarie, K., Chao, D., Kitzis, D., Novelli, P., Zhao, C., et al.: CO 2, CO, and CH 4 measurements from tall towers in the NOAA Earth System Research Laboratory's Global Greenhouse Gas Reference Network: Instrumentation, uncertainty analysis, and recommendations for future high-accuracy greenhouse gas monitoring efforts, Atmospheric Measurement Techniques, 7, 647–687, 2014.

Arevalo-Martínez, D. L., Kock, A., Löscher, C., Schmitz, R. A., and Bange, H. W.: Massive nitrous oxide emissions from the tropical South Pacific Ocean, Nature Geoscience, 8, 530–533, 2015.

Babbin, A. R., Bianchi, D., Jayakumar, A., and Ward, B. B.: Rapid nitrous oxide cycling in the suboxic ocean, Science, 348, 1127–1129, 2015.

Babbin, A. R., Boles, E. L., Mühle, J., and Weiss, R. F.: On the natural spatio-temporal heterogeneity of South Pacific nitrous oxide, Nature Communications, 11, 3672, 2020.

Bange, H. W., Rapsomanikis, S., and Andreae, M. O.: Nitrous oxide in coastal waters, Global Biogeochemical Cycles, 10, 197–207, 1996.

Bange, H. W., Arévalo-Martínez, D. L., De La Paz, M., Farías, L., Kaiser, J., Kock, A., Law, C. S., Rees, A. P., Rehder, G., Tortell, P. D., et al.: A harmonized nitrous oxide (N2O) ocean observation network for the 21st century, Frontiers in Marine Science, 6, 157, 2019.

Bray, C. D., Battye, W. H., Aneja, V. P., and Schlesinger, W. H.: Global emissions of NH3, NOx, and N2O from biomass burning and the impact of climate change, Journal of the Air & Waste Management Association, 71, 102–114, 2021.

Buitenhuis, E. T., Suntharalingam, P., and Le Quéré, C.: Constraints on global oceanic emissions of N 2 O from observations and models, Biogeosciences, 15, 2161–2175, 2018.

Canadell, J. G., Monteiro, P. M., Costa, M. H., Da Cunha, L. C., Cox, P. M., Eliseev, A. V., Henson, S., Ishii, M., Jaccard, S., Koven, C., Lohila, A., Patra, P. K., Piao, S., Rogelj, J., Syampungani, S., Zaehle, S., and Zickfeld, K.: Global Carbon and other Biogeochemical Cycles and Feedbacks, in: Climate Change 2021: The Physical Science Basis. Contribution of Working Group I to the Sixth Assessment Report of the Intergovernmental Panel on Climate Change, Cambridge University Press, 2021.

Cazorla, M. and Herrera, E.: Air quality in the Galapagos Islands: A baseline view from remote sensing and in situ measurements, Meteorological Applications, 27, e1878, 2020.

Cofer III, W., Levine, J., Winstead, E., and Stocks, B.: New estimates of nitrous oxide emissions from biomass burning, Nature, 349, 689–691, 1991.

Dutton, G., Hall, B., Dlugokencky, E., Lan, X., Nance, J., and Madronich, M.: Combined Atmospheric Nitrous Oxide Dry Air Mole Fractions from the NOAA GML Halocarbons Sampling Network, 1977–2024, Version: 2024-02-21, NOAA, 2024.

Forryan, A., Naveira Garabato, A. C., Vic, C., Nurser, A. G., and Hearn, A. R.: Galápagos upwelling driven by localized wind–front interactions, Scientific Reports, 11, 1277, 2021.

Forster, P., Storelvmo, T., Armour, K., Collins, W., Dufresne, J.-L., Frame, D., Lunt, D., Mauritsen, T., Palmer, M., Watanabe, M., Wild, M., and Zhang, H.: The Earth's energy budget, climate feedbacks, and climate sensitivity, in: Climate Change 2021: The Physical Science Basis. Contribution of Working Group I to the Sixth Assessment Report of the Intergovernmental Panel on Climate Change, Cambridge University Press, 2021.

https://doi.org/10.5194/egusphere-2024-3769
Preprint. Discussion started: 17 December 2024

Francey, R., Steele, L., Spencer, D., Langenfelds, R., Law, R., Krummel, P., Fraser, P., Etheridge, D., Derek, N., Coram, S., et al.: The CSIRO (Australia) measurement of greenhouse gases in the global atmosphere, Baseline Atmospheric Program Australia, edited by: Tindale, NW, Derek, N., and Fraser, PJ, Bureau of Meteorology and CSIRO Atmospheric Research, Melbourne, pp. 42–53, 2003.

Ganesan, A., Chatterjee, A., Prinn, R., Harth, C., Salameh, P., Manning, A., Hall, B., Mühle, J., Meredith, L., Weiss, R., et al.: The variability of methane, nitrous oxide and sulfur hexafluoride in Northeast India, Atmospheric Chemistry and Physics, 13, 10 633–10 644, 2013.

Ganesan, A., Manning, A., Grant, A., Young, D., Oram, D., Sturges, W., Moncrieff, J., and O'Doherty, S.: Quantifying methane and nitrous oxide emissions from the UK and Ireland using a national-scale monitoring network, Atmospheric Chemistry and Physics, 15, 6393–6406, 2015.

Ganesan, A. L., Manizza, M., Morgan, E., Harth, C., Kozlova, E., Lueker, T., Manning, A., Lunt, M., Mühle, J., Lavric, J., et al.: Marine nitrous oxide emissions from three eastern boundary upwelling systems inferred from atmospheric observations, Geophysical Research Letters, 47, e2020GL087 822, 2020.

Gómez Martín, J. C., Mahajan, A. S., Hay, T. D., Prados-Román, C., Ordóñez, C., MacDonald, S. M., Plane, J. M., Sorribas, M., Gil, M., Paredes Mora, J. F., et al.: Iodine chemistry in the eastern Pacific marine boundary layer, Journal of Geophysical Research: Atmospheres, 118, 887–904, 2013.

Grant, A., Witham, C., Simmonds, P., Manning, A., and O'Doherty, S.: A 15 year record of high-frequency, in situ measurements of hydrogen at Mace Head, Ireland, Atmospheric Chemistry and Physics, 10, 1203–1214, 2010.

Griffis, T., Lee, X., Baker, J., Russelle, M., Zhang, X., Venterea, R., and Millet, D.: Reconciling the differences between top-down and bottom-up estimates of nitrous oxide emissions for the US Corn Belt, Global Biogeochemical Cycles, 27, 746–754, 2013.

Hall, B., Dutton, G., and Elkins, J.: The NOAA nitrous oxide standard scale for atmospheric observations, Journal of Geophysical Research: Atmospheres, 112, 2007.

Henne, S., Brunner, D., Oney, B., Leuenberger, M., Eugster, W., Bamberger, I., Meinhardt, F., Steinbacher, M., and Emmenegger, L.: Validation of the Swiss methane emission inventory by atmospheric observations and inverse modelling, Atmospheric Chemistry and Physics, 16, 3683–3710, 2016.

Hersbach, H., Bell, B., Berrisford, P., Biavati, G., Horányi, A., Muñoz Sabater, J., Nicolas, J., Peubey, C., Radu, R., Rozum, I., Schepers, D., Simmons, A., Soci, C., Dee, D., and Thépaut, J.-N.: ERA5 hourly data on pressure levels from 1940 to present, Copernicus Climate Change Service (C3S) Climate Data Store (CDS), https://doi.org/10.24381/cds.bd0915c6, 2023.

Hirsch, A., Michalak, A., Bruhwiler, L., Peters, W., Dlugokencky, E., and Tans, P.: Inverse modeling estimates of the global nitrous oxide surface flux from 1998–2001, Global Biogeochemical Cycles, 20, 2006.

Jeong, S., Newman, S., Zhang, J., Andrews, A. E., Bianco, L., Dlugokencky, E., Bagley, J., Cui, X., Priest, C., Campos-Pineda, M., et al.: Inverse estimation of an annual Cycle of California's nitrous oxide emissions, Journal of Geophysical Research: Atmospheres, 123, 4758–4771, 2018.

Ji, Q., Altabet, M. A., Bange, H. W., Graco, M. I., Ma, X., Arévalo-Martínez, D. L., and Grundle, D. S.: Investigating the effect of El Niño on nitrous oxide distribution in the eastern tropical South Pacific, Biogeosciences, 16, 2079–2093, 2019.

Labuschagne, C., Kuyper, B., Brunke, E.-G., Mokolo, T., Van der Spuy, D., Martin, L., Mbambalala, E., Parker, B., Khan, M. A. H., Davies-Coleman, M. T., et al.: A review of four decades of atmospheric trace gas measurements at Cape Point, South Africa, Transactions of the Royal Society of South Africa, 73, 113–132, 2018.

https://doi.org/10.5194/egusphere-2024-3769
Preprint. Discussion started: 17 December 2024

Lan, X., Mund, J., Crotwell, A., Thoning, K., Moglia, E., Madronich, M., Baugh, K., Petron, G., Crotwell, M., Neff, D., Wolter, S., Mefford, T., and DeVogel, S.: Atmospheric Nitrous Oxide Dry Air Mole Fractions from the NOAA GML Carbon Cycle Cooperative Global Air Sampling Network, https://doi.org/10.15138/53g1-x417, 1997-2023, Version: 2024-07-30, 2024.

Landolfi, A., Somes, C. J., Koeve, W., Zamora, L. M., and Oschlies, A.: Oceanic nitrogen cycling and N2O flux perturbations in the Anthropocene, Global Biogeochemical Cycles, 31, 1236–1255, 2017.

Lebegue, B., Schmidt, M., Ramonet, M., Wastine, B., Yver Kwok, C., Laurent, O., Belviso, S., Guemri, A., Philippon, C., Smith, J., et al.: Comparison of nitrous oxide (N 2 O) analyzers for high-precision measurements of atmospheric mole fractions, Atmospheric Measurement Techniques, 9, 1221–1238, 2016.

Lunt, M. F., Manning, A. J., Allen, G., Arnold, T., Bauguitte, S. J.-B., Boesch, H., Ganesan, A. L., Grant, A., Helfter, C., Nemitz, E., et al.: Atmospheric observations consistent with reported decline in the UK's methane emissions (2013–2020), Atmospheric Chemistry and Physics, 21, 16 257–16 276, 2021.

Martinez-Rey, J., Bopp, L., Gehlen, M., Tagliabue, A., and Gruber, N.: Projections of oceanic N 2 O emissions in the 21st century using the IPSL Earth system model, Biogeosciences, 12, 4133–4148, 2015.

Mateus, C., Flor, D., Guerrero, C. A., Córdova, X., Benitez, F. L., Parra, R., and Ochoa-Herrera, V.: Anthropogenic emission inventory and spatial analysis of greenhouse gases and primary pollutants for the Galapagos Islands, Environmental Science and Pollution Research, 30, 68 900–68 918, 2023.

McCoy, D., Damien, P., Clements, D., Yang, S., and Bianchi, D.: Pathways of nitrous oxide production in the eastern tropical south pacific oxygen minimum zone, Global Biogeochemical Cycles, 37, e2022GB007 670, 2023.

Nevison, C., Andrews, A., Thoning, K., Dlugokencky, E., Sweeney, C., Miller, S., Saikawa, E., Benmergui, J., Fischer, M., Mountain, M., et al.: Nitrous oxide emissions estimated with the CarbonTracker-Lagrange North American regional inversion framework, Global Biogeochemical Cycles, 32, 463–485, 2018.

Nevison, C., Lan, X., and Ogle, S. M.: Remote sensing soil freeze-thaw status and North American N2O emissions from a regional inversion, Global Biogeochemical Cycles, 37, e2023GB007 759, 2023.

Nevison, C. D., Weiss, R. F., and Erickson III, D. J.: Global oceanic emissions of nitrous oxide, Journal of Geophysical Research: Oceans, 100, 15 809–15 820, 1995.

Novelli, P. C., Elkins, J. W., and Steele, L. P.: The development and evaluation of a gravimetric reference scale for measurements of atmospheric carbon monoxide, Journal of Geophysical Research: Atmospheres, 96, 13 109–13 121, 1991.

Paltán, H. A., Benitez, F. L., Rosero, P., Escobar-Camacho, D., Cuesta, F., and Mena, C. F.: Climate and sea surface trends in the Galapagos Islands, Scientific Reports, 11, 14 465, 2021.

Patra, P. K., Dlugokencky, E. J., Elkins, J. W., Dutton, G. S., Tohjima, Y., Sasakawa, M., Ito, A., Weiss, R. F., Manizza, M., Krummel, P. B., et al.: Forward and inverse modelling of atmospheric nitrous oxide using MIROC4-atmospheric chemistry-transport model, Journal of the Meteorological Society of Japan. Ser. II, 100, 361–386, 2022.

Pisso, I., Sollum, E., Grythe, H., Kristiansen, N. I., Cassiani, M., Eckhardt, S., Arnold, D., Morton, D., Thompson, R. L., Groot Zwaaftink, C. D., et al.: The Lagrangian particle dispersion model FLEXPART version 10.4, Geoscientific Model Development, 12, 4955–4997, 2019.

Prather, M. J., Hsu, J., DeLuca, N. M., Jackman, C. H., Oman, L. D., Douglass, A. R., Fleming, E. L., Strahan, S. E., Steenrod, S. D., Søvde, O. A., et al.: Measuring and modeling the lifetime of nitrous oxide including its variability, Journal of Geophysical Research: Atmospheres, 120, 5693–5705, 2015.

https://doi.org/10.5194/egusphere-2024-3769
Preprint. Discussion started: 17 December 2024

Prinn, R. G., Weiss, R. F., Arduini, J., Arnold, T., DeWitt, H. L., Fraser, P. J., Ganesan, A. L., Gasore, J., Harth, C. M., Hermansen, O., et al.: History of chemically and radiatively important atmospheric gases from the Advanced Global Atmospheric Gases Experiment (AGAGE), Earth System Science Data, 10, 985–1018, 2018.

Ravishankara, A., Daniel, J. S., and Portmann, R. W.: Nitrous oxide (N2O): the dominant ozone-depleting substance emitted in the 21st century, science, 326, 123–125, 2009.

Rella, C.: Accurate greenhouse gas measurements in humid gas streams using the Picarro G1301 carbon dioxide/methane/water vapor gas analyzer, White paper, Picarro Inc, Sunnyvale, CA, USA, 2010.

Resplandy, L., Hogikyan, A., Müller, J. D., Najjar, R., Bange, H. W., Bianchi, D., Weber, T., Cai, W.-J., Doney, S., Fennel, K., et al.: A synthesis of global coastal ocean greenhouse gas fluxes, Global biogeochemical cycles, 38, e2023GB007 803, 2024.

Reum, F., Gerbig, C., Lavric, J. V., Rella, C. W., and Göckede, M.: Correcting atmospheric CO 2 and CH 4 mole fractions obtained with Picarro analyzers for sensitivity of cavity pressure to water vapor, Atmospheric Measurement Techniques, 12, 1013–1027, 2019.

Risien, C. M. and Chelton, D. B.: A global climatology of surface wind and wind stress fields from eight years of QuikSCAT scatterometer data, Journal of Physical Oceanography, 38, 2379–2413, 2008.

Saboya, E., Manning, A. J., Levy, P., Stanley, K. M., Pitt, J., Young, D., Say, D., Grant, A., Arnold, T., Rennick, C., et al.: Combining top-down and bottom-up approaches to evaluate recent trends and seasonal patterns in UK N2O emissions, Journal of Geophysical Research: Atmospheres, 129, e2024JD040 785, 2024.

Saikawa, E., Prinn, R., Dlugokencky, E., Ishijima, K., Dutton, G., Hall, B., Langenfelds, R., Tohjima, Y., Machida, T., Manizza, M., et al.: Global and regional emissions estimates for N 2 O, Atmospheric Chemistry and Physics, 14, 4617–4641, 2014.

Seibert, P. and Frank, A.: Source-receptor matrix calculation with a Lagrangian particle dispersion model in backward mode, Atmospheric Chemistry and Physics, 4, 51–63, 2004.

Sorribas, M., Martín, J. G., Hay, T., Mahajan, A. S., Cuevas, C. A., Reyes, M. A., Mora, F. P., Gil-Ojeda, M., and Saiz-Lopez, A.: On the concentration and size distribution of sub-micron aerosol in the Galápagos Islands, Atmospheric Environment, 123, 39–48, 2015.

Stanley, K. M., Grant, A., O'Doherty, S., Young, D., Manning, A. J., Stavert, A. R., Spain, T. G., Salameh, P. K., Harth, C. M., Simmonds, P. G., et al.: Greenhouse gas measurements from a UK network of tall towers: technical description and first results, Atmospheric Measurement Techniques, 11, 1437–1458, 2018.

Stavert, A. R., O'doherty, S., Stanley, K., Young, D., Manning, A. J., Lunt, M. F., Rennick, C., and Arnold, T.: UK greenhouse gas measurements at two new tall towers for aiding emissions verification, Atmospheric Measurement Techniques, 12, 4495–4518, 2019.

Stell, A. C., Bertolacci, M., Zammit-Mangion, A., Rigby, M., Fraser, P. J., Harth, C. M., Krummel, P. B., Lan, X., Manizza, M., Mühle, J., et al.: Modelling the growth of atmospheric nitrous oxide using a global hierarchical inversion, Atmospheric Chemistry and Physics, 22, 12 945–12 960, 2022.

Stohl, A., Hittenberger, M., and Wotawa, G.: Validation of the Lagrangian particle dispersion model FLEXPART against large-scale tracer experiment data, Atmospheric Environment, 32, 4245–4264, 1998.

Stohl, A., Forster, C., Frank, A., Seibert, P., and Wotawa, G.: The Lagrangian particle dispersion model FLEXPART version 6.2, Atmospheric Chemistry and Physics, 5, 2461–2474, 2005.

Stohl, A., Seibert, P., Arduini, J., Eckhardt, S., Fraser, P., Greally, B., Lunder, C., Maione, M., Mühle, J., O'doherty, S., et al.: An analytical inversion method for determining regional and global emissions of greenhouse gases: Sensitivity studies and application to halocarbons, Atmospheric Chemistry and Physics, 9, 1597–1620, 2009.

https://doi.org/10.5194/egusphere-2024-3769
Preprint. Discussion started: 17 December 2024

Stramma, L., Johnson, G. C., Sprintall, J., and Mohrholz, V.: Expanding oxygen-minimum zones in the tropical oceans, science, 320, 655–658, 2008.

Suntharalingam, P., Sarmiento, J. L., and Toggweiler, J.: Global significance of nitrous-oxide production and transport from oceanic low-oxygen zones: A modeling study, Global Biogeochemical Cycles, 14, 1353–1370, 2000.

Thompson, R., Manning, A., Gloor, E., Schultz, U., Seifert, T., Hänsel, F., Jordan, A., and Heimann, M.: In-situ measurements of oxygen, carbon monoxide and greenhouse gases from Ochsenkopf tall tower in Germany, Atmospheric Measurement Techniques, 2, 573–591, 2009.

Thompson, R., Dlugokencky, E., Chevallier, F., Ciais, P., Dutton, G., Elkins, J., Langenfelds, R., Prinn, R., Weiss, R., Tohjima, Y., et al.: Interannual variability in tropospheric nitrous oxide, Geophysical research letters, 40, 4426–4431, 2013.

Thompson, R. L., Chevallier, F., Crotwell, A. M., Dutton, G., Langenfelds, R. L., Prinn, R. G., Weiss, R. F., Tohjima, Y., Nakazawa, T., Krummel, P. B., et al.: Nitrous oxide emissions 1999 to 2009 from a global atmospheric inversion, Atmospheric Chemistry and Physics, 14, 1801–1817, 2014.

Thompson, R. L., Lassaletta, L., Patra, P. K., Wilson, C., Wells, K. C., Gressent, A., Koffi, E. N., Chipperfield, M. P., Winiwarter, W., Davidson, E. A., et al.: Acceleration of global N2O emissions seen from two decades of atmospheric inversion, Nature Climate Change, 9, 993–998, 2019.

Tian, H., Pan, N., Thompson, R. L., Canadell, J. G., Suntharalingam, P., Regnier, P., Davidson, E. A., Prather, M., Ciais, P., Muntean, M., Pan, S., Winiwarter, W., Zaehle, S., Zhou, F., Jackson, R. B., Bange, H. W., Berthet, S., Bian, Z., Bianchi, D., Bouwman, A. F., Buitenhuis, E. T., Dutton, G., Hu, M., Ito, A., Jain, A. K., Jeltsch-Thömmes, A., Joos, F., Kou-Giesbrecht, S., Krummel, P. B., Lan, X., Landolfi, A., Lauerwald, R., Li, Y., Lu, C., Maavara, T., Manizza, M., Millet, D. B., Mühle, J., Patra, P. K., Peters, G. P., Qin, X., Raymond, P., Resplandy, L., Rosentreter, J. A., Shi, H., Sun, Q., Tonina, D., Tubiello, F. N., van der Werf, G. R., Vuichard, N., Wang, J., Wells, K. C., Western, L. M., Wilson, C., Yang, J., Yao, Y., You, Y., and Zhu, Q.: Global nitrous oxide budget (1980–2020), Earth System Science Data, 16, 2543–2604, https://doi.org/10.5194/essd-16-2543-2024, 2024.

Tohjima, Y., Machida, T., Utiyama, M., Katsumoto, M., Fujinuma, Y., and Maksyutov, S.: Analysis and presentation of in situ atmospheric methane measurements from Cape Ochi-ishi and Hateruma Island, Journal of Geophysical Research: Atmospheres, 107, ACH–8, 2002.

Watson, C. E., Fishman, J., and Reichle Jr, H. G.: The significance of biomass burning as a source of carbon monoxide and ozone in the southern hemisphere tropics: A satellite analysis, Journal of Geophysical Research: Atmospheres, 95, 16 443–16 450, 1990.

Wells, K. C., Millet, D. B., Bousserez, N., Henze, D., Chaliyakunnel, S., Griffis, T. J., Luan, Y., Dlugokencky, E., Prinn, R., O'Doherty, S., et al.: Simulation of atmospheric N 2 O with GEOS-Chem and its adjoint: evaluation of observational constraints, Geoscientific Model Development, 8, 3179–3198, 2015.

Wells, K. C., Millet, D. B., Bousserez, N., Henze, D. K., Griffis, T. J., Chaliyakunnel, S., Dlugokencky, E. J., Saikawa, E., Xiang, G., Prinn, R. G., et al.: Top-down constraints on global N 2 O emissions at optimal resolution: application of a new dimension reduction technique, Atmospheric Chemistry and Physics, 18, 735–756, 2018.

Welp, L., Keeling, R., Weiss, R., Paplawsky, W., and Heckman, S.: Design and performance of a Nafion dryer for continuous operation at CO 2 and CH 4 air monitoring sites, Atmospheric Measurement Techniques, 6, 1217–1226, 2013.

Wilson, S., Dick, A., Fraser, P., and Whittlestone, S.: Nitrous oxide flux estimates for south-eastern Australia, Journal of Atmospheric Chemistry, 26, 169–188, 1997.

https://doi.org/10.5194/egusphere-2024-3769
Preprint. Discussion started: 17 December 2024

Yang, S., Chang, B. X., Warner, M. J., Weber, T. S., Bourbonnais, A. M., Santoro, A. E., Kock, A., Sonnerup, R. E., Bullister, J. L., Wilson, S. T., et al.: Global reconstruction reduces the uncertainty of oceanic nitrous oxide emissions and reveals a vigorous seasonal cycle, Proceedings of the National Academy of Sciences, 117, 11 954–11 960, 2020.

Zellweger, C., Steinbrecher, R., Laurent, O., Lee, H., Kim, S., Emmenegger, L., Steinbacher, M., and Buchmann, B.: Recent advances in measurement techniques for atmospheric carbon monoxide and nitrous oxide observations, Atmospheric Measurement Techniques, 12, 5863–5878, 2019.

Zhang, F., Zhou, L., Novelli, P., Worthy, D., Zellweger, C., Klausen, J., Ernst, M., Steinbacher, M., Cai, Y., Xu, L., et al.: Evaluation of in situ measurements of atmospheric carbon monoxide at Mount Waliguan, China, Atmospheric Chemistry and Physics, 11, 5195–5206, 2011.

Zhang, X., Lee, X., Griffis, T. J., Baker, J. M., and Xiao, W.: Estimating regional greenhouse gas fluxes: an uncertainty analysis of planetary boundary layer techniques and bottom-up inventories, Atmospheric chemistry and physics, 14, 10 705–10 719, 2014.